

# Insights into peptide nucleic acid (PNA) structural features: The crystal structure of a D-lysine-based chiral PNA–DNA duplex

Valeria Menchise\*, Giuseppina De Simone\*, Tullia Tedeschi†, Roberto Corradini†, Stefano Sforza†, Rosangela Marchelli†‡, Domenica Capasso\*, Michele Saviano\*, and Carlo Pedone\*‡

\*Istituto di Biostrutture e Bioimmagini, Consiglio Nazionale delle Ricerche, Via Mezzocannone 6, I-80134 Naples, Italy; and †Dipartimento di Chimica Organica e Industriale, University of Parma, Area Parco delle Scienze 17/A, I-43100 Parma, Italy

Communicated by Isabella L. Karle, Naval Research Laboratory, Washington, DC, July 28, 2003 (received for review April 10, 2003)

Peptide nucleic acids (PNAs) are oligonucleotide analogues in which the sugar-phosphate backbone has been replaced by a pseudopeptide skeleton. They bind DNA and RNA with high specificity and selectivity, leading to PNA–RNA and PNA–DNA hybrids more stable than the corresponding nucleic acid complexes. The binding affinity and selectivity of PNAs for nucleic acids can be modified by the introduction of stereogenic centers (such as D-Lys-based units) into the PNA backbone. To investigate the structural features of chiral PNAs, the structure of a PNA decamer containing three D-Lys-based monomers (namely H-GpnTpnApnGpnAdlTdlCdlApnCpnTpn-NH<sub>2</sub>, in which pn represents a pseudopeptide link and dl represents a D-Lys analogue) hybridized with its complementary antiparallel DNA has been solved at a 1.66-Å resolution by means of a single-wavelength anomalous diffraction experiment on a brominated derivative. The D-Lys-based chiral PNA–DNA (LPD) heteroduplex adopts the so-called P-helix conformation. From the substantial similarity between the PNA conformation in LPD and the conformations observed in other PNA structures, it can be concluded that PNAs possess intrinsic conformational preferences for the P-helix, and that their flexibility is rather restricted. The conformational rigidity of PNAs is enhanced by the presence of the chiral centers, limiting the ability of PNA strands to adopt other conformations and, ultimately, increasing the selectivity in molecular recognition.

Peptide nucleic acids (PNAs) are oligonucleotide mimics in which the sugar-phosphate backbone has been replaced by a pseudopeptide skeleton, composed of *N*-(2-aminoethyl)glycine units (1) (Fig. 1). Nucleobases are linked to this skeleton through a two-atom carboxymethyl spacer.

PNAs bind DNA and RNA with high specificity and selectivity, forming Watson–Crick base pairs and leading to PNA–RNA and PNA–DNA hybrids that are more stable than the corresponding nucleic acid complexes (2). Because of their high thermal stability and resistance to proteases and nucleases, PNAs are ideal candidates as antisense or antigene therapeutic agents (3–6) and are currently used as powerful tools in molecular biology and in diagnostics (7).

Three-dimensional structures have been determined for the major families of PNA complexes by different techniques. A PNA–RNA duplex (8) and a PNA–DNA duplex (9) were characterized by NMR in solution, whereas a (PNA)<sub>2</sub>–DNA triplex (10) and three PNA–PNA duplexes (11–13) were solved by x-ray crystallography. The structural analysis in solution of the PNA–DNA (9) and PNA–RNA duplexes (8) showed that PNA, when hybridized to RNA, adopts an A-like helix, whereas, when hybridized to a complementary DNA strand, it adopts a conformation that is different from both the A and the B forms. The crystal structure of the (PNA)<sub>2</sub>–DNA triplex (10) also showed helical parameters significantly different from those of canonical DNA or RNA helical forms, defining a type of helix, named the P-helix, characterized by a small twist angle, a large x-displacement, and a wide, deep major groove. Finally, structural features of the PNA–PNA double helix (11–13) are similar to those of the P-helix mentioned above.

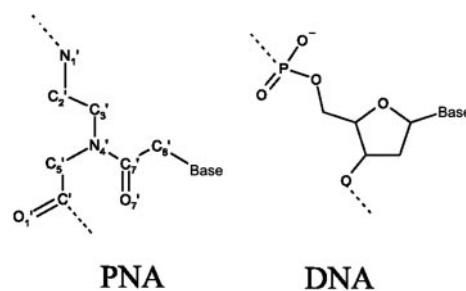


Fig. 1. Chemical structures of PNA and DNA oligomers.

PNAs can bind to complementary DNA strands in both parallel and antiparallel orientations and are poorly soluble under physiological conditions, thus preventing the development of PNA-based therapeutics (14–15). To improve binding specificity, solubility, and uptake into cells (16), several modifications of the basic PNA structure have been proposed. A particular approach involves the introduction of stereogenic centers, most commonly based on chiral aminoethyl amino acids (17). Circular dichroism experiments have demonstrated that the configuration of the stereogenic centers induces preferential PNA helicity; in particular, PNAs containing monomers derived from D-amino acids (D-PNAs) induce a preferred right-handedness in the PNA–PNA duplexes, whereas L-PNAs induce left-handedness (18–19). As a consequence of this preferential handedness, right-handed DNA was found to bind to D-PNAs with higher affinity than L-PNAs (18).

Chiral PNAs were found to form slightly less stable PNA–DNA duplexes than their achiral analogues, the effect being more pronounced for backbones containing amino acids with bulky apolar side chains. Negatively charged monomers (based on either D- or L-aspartic and glutamic acids) were shown to destabilize PNA–DNA duplexes even more, probably on account of the repulsive interactions with the negatively charged phosphate groups of the DNA. On the other hand, by introducing positively charged Lys-based monomers, more stable PNA–DNA duplexes were obtained (17). On the basis of these results, recently Sforza *et al.* (20) reported the synthesis of a chiral PNA decamer containing three adjacent chiral monomers based on D-Lys (chiral box) in the middle of the PNA sequence (H-GpnTpnApnGpnAdlTdlCdlApnCpnTpn-NH<sub>2</sub>; Fig. 24), which was shown to hybridize with the complementary DNA sequence only in the antiparallel mode. Furthermore, the

Abbreviations: PNA, peptide nucleic acid; pn, pseudopeptide link; dl, D-Lys analogue; LPD, D-Lys-based chiral PNA–DNA.

Data deposition: The atomic coordinates and structure factors have been deposited in the Protein Data Bank, www.rcsb.org (PDB ID code 1NR8).

†To whom correspondence may be addressed. E-mail: rosangela.marchelli@unipr.it or pedone@chemistry.unina.it.

© 2003 by The National Academy of Sciences of the USA

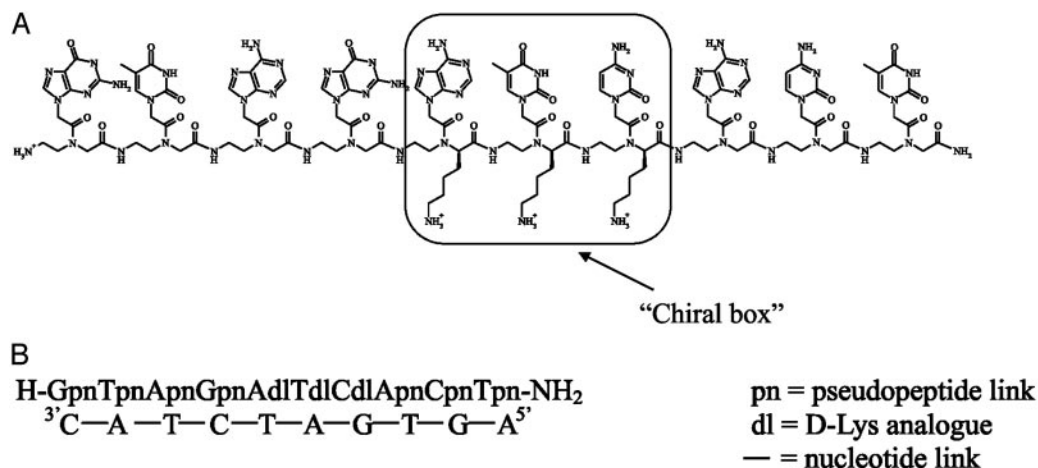


**Fig. 2.** (A) The PNA sequence containing three D-Lys-based PNA monomers (chiral box). (B) The PNA decamer containing the chiral box hybridized with its complementary antiparallel DNA strand.

single mismatch recognition was greatly enhanced relative to that observed for other achiral or chiral PNAs (20). Thus, the PNA containing the chiral box is endowed with many of the properties required for detection of point mutations in diagnostics and for selective binding in therapeutics.

In a general research project aimed at understanding the role of chirality in DNA recognition and at achieving insights into the structure–activity relationships of chiral PNAs, we have succeeded in crystallizing the PNA decamer containing the chiral box hybridized with its complementary antiparallel DNA strand (Fig. 2B) (21). Here, we report the crystal structure of the duplex at a 1.66-Å resolution solved by a single-wavelength anomalous diffraction experiment on a brominated derivative.

## Methods

### Synthesis of the PNA Strand, Crystallization, and Data Collection.

Synthesis of the D-Lys-based PNA was carried out by a submonomeric approach to obtain high optical purity (enantiomeric excess = 94.4%), as described elsewhere (22).

Preparation and crystallization of the double strand PNA–DNA by using PEG 8000 as precipitant and cacodylate at pH 6.3 have already been reported (21). A native data set at a 1.66-Å resolution was collected at the European Synchrotron Radiation Facility (Grenoble, France) by using one crystal, flash cooled to 100 K, from a precipitant solution containing 10% glycerol. Crystals belong to space group  $P3_1$  with one molecule per asymmetric unit.

To determine the structure by a single-wavelength anomalous diffraction experiment, a DNA strand containing two 5-BrUra moieties (BrU) (AG<sup>Br</sup>UGATC<sup>Br</sup>UAC) was synthesized and a Br-derivative PNA–DNA duplex was prepared. Crystals of the Br-derivative were grown by the hanging-drop vapor diffusion method at 20°C, setting up 2  $\mu$ l of duplex solution with 2  $\mu$ l of reservoir solution, consisting of 15% 2-propanol, 50 mM Mes (pH 6.0), and 20 mM magnesium chloride. Several macroseeding experiments were necessary to obtain single crystals of dimensions 0.04  $\times$  0.04  $\times$  0.5 mm<sup>3</sup>. Crystals were isomorphous with native crystals. Single-wavelength anomalous diffraction data at a 1.75-Å resolution were collected around the absorption Br K edge on a Mar charge-coupled device detector at the Elettra Synchrotron source in Trieste, by using one crystal flash cooled at 100 K from a precipitant solution containing 15% glycerol.

The data sets of the native and Br-derivative PNA–DNA were processed by using the HKL crystallographic data reduction package (DENZO/SCALEPACK) (23). The statistics of data collections are given in Table 1.

**Structure Determination and Refinement.** Determination and refinement of the two bromide sites and phase calculations were carried out with the program SOLVE (24), using data between a 20.0- and

**Table 1.** Data collection, phasing, and refinement statistics

	Native	5-BrUra
<b>Crystal data</b>		
Space group	$P3_1$	$P3_1$
<i>a</i> , Å	34.94	34.97
<i>c</i> , Å	35.80	35.92
Independent molecules	1	1
<b>Diffraction data</b>		
Wavelength, Å	1.200	0.918
Resolution limits, Å	20.0–1.66	20.0–1.75
Total reflections	46,117	94,574
Unique reflections	5,617	4,831
Completeness, %		
Overall	97.8	100.0
Outermost data shell	95.1	100.0
<i>I</i> / $\sigma$ ( <i>I</i> )		
Overall	15.4	21.2
Outermost data shell	5.1	11.4
<i>R</i> <sub>merge</sub> , %*		
Overall	6.0	10.6
Outermost data shell	18.5	20.4
<b>Phasing</b>		
Resolution, Å		20–2.0
Overall figure of merit		0.40 (0.76 after DM)
<b>Refinement</b>		
Reflections used	5,429	
Resolution, Å	20–1.66	
<i>R</i> <sub>factor</sub> , % <sup>†</sup>	19.7	
<i>R</i> <sub>free</sub> , % <sup>‡</sup>	22.8	
rms deviation from ideal geometry		
Bond length, Å	0.011	
Bond angles, °	1.1	
Average <i>B</i> factor, Å <sup>2</sup>		
Overall	26.12	
PNA strand	22.35	
DNA strand	25.65	
Water molecules	37.06	

\**R*<sub>merge</sub> =  $\sum |I| - I / \sum I$  over all reflections.

<sup>†</sup>*R*<sub>factor</sub> =  $\sum |F_o - F_c| / \sum F_o$ .

<sup>‡</sup>*R*<sub>free</sub> was calculated with 10% of data withheld from refinement.

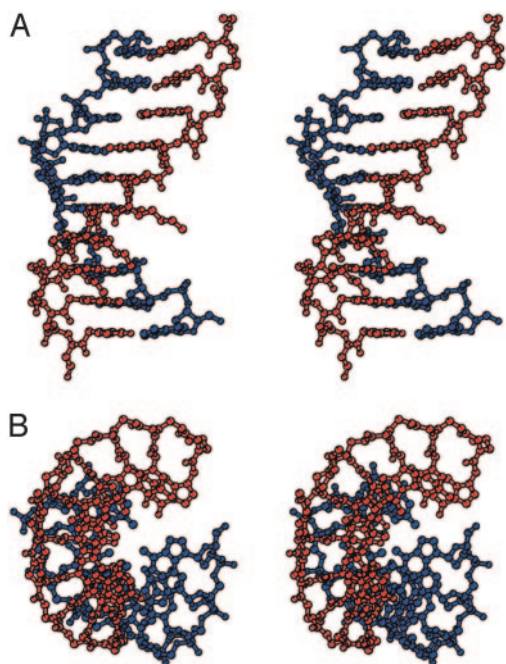


**Fig. 3.** (A) Stereoview of D-Lys-based chiral PNA–DNA double-helix structure. (B) View down the helical axis. The DNA strand is shown in blue, and the PNA strand is shown in red. The image was generated by using BOBSCRIPT (38).

a 2.0-Å resolution. The initial density map, calculated at 2.0 Å and weighted by a figure of merit of 0.40, was improved by density modification and phases were extended by using DM (25, 26). At this stage, the nucleobases and clear duplex–solvent boundaries were discerned within the map. Starting at the bromide sites, a partial model was built with the program O (27). Iterative phase combinations using SIGMAA (25, 28) were repeated until all of the nucleobases and the backbone were fitted into the electron density.

The structure was then refined against the native data set by using CNS (29). Several cycles of simulated annealing, minimization, and B factor refinement, followed by manual model rebuilding with O, reduced the  $R_{\text{factor}}$  and  $R_{\text{free}}$  values for all of the data in the resolution range from 20.0–1.66 Å to 0.197 and 0.228, respectively. Statistics of structure determination and refinement are given in Table 1.

## Results

**Quality of the Model.** D-Lys-based chiral PNA was obtained by a submonomeric synthesis at high optical purity (22). Crystals of the D-Lys-based chiral PNA–DNA (LPD) duplex, diffracting at a 1.66-Å resolution, were obtained as described (21). The structure of

the duplex was solved by a single wavelength anomalous diffraction experiment on a brominated derivative and refined to an  $R_{\text{factor}}$  of 19.7% and  $R_{\text{free}}$  of 22.8%, using 5,429 reflections in the 20.0- to 1.66-Å resolution range.

The final model consists of 413 nonhydrogen atoms, 80 water molecules, and 1 magnesium ion derived from the crystallization solution. Both the nucleobases and the PNA and DNA backbones are very well defined in the electron density maps. The refined structure presents a good geometry with root mean square deviations from ideal bond lengths and angles of 0.011 Å and 1.1°, respectively. The average temperature factor ( $B$ ) for all atoms is 26.12 Å<sup>2</sup> (see Table 1).

**Overall Structure.** The LPD duplex forms an antiparallel right-handed double helix with a diameter of  $\approx 22$  Å, an average helical twist of 23.2°, a rise of 3.5 Å, and 16 base pairs per turn (30, 31) (Fig. 3, Tables 2 and 3). This helix presents a large cavity along the helical axis as indicated by a base pair  $x$ -displacement of  $-3.8$  Å. All these features correlate with a double helix with a very wide and deep major groove and a narrow and shallow minor groove.

All of the bases are engaged in Watson–Crick hydrogen bonds (Fig. 4A). The pattern of the base stacking resembles that found in the B form of the DNA double helix with the base pairs nearly perpendicular to the helical axis. A continuous base pair stacking is formed between symmetry-related helices. In particular at the intermolecular interface the nucleobase of PNA residue Gpn1 stacks with the nucleobase of DNA residue A1, whereas the nucleobase of DNA residue C10 stacks with the nucleobase of PNA residue Tpn10 (Fig. 5A).

DNA backbone torsion angles are reported in Table 4. These values are close to those of A-type DNA, with *anti* glycosidic torsion angles, except for the  $\delta$  and  $\chi$  angles. The latter parameters, particularly evident in the  $\delta$  angle, are more A-like for the first six nucleotides and more B-like for the last four. These findings are correlated with differences observed in the conformation of the sugar moieties along the sequence (Table 4). In particular the puckering of the sugar rings is C3'-*endo* (as in A-DNA) in the first six units and C2'-*endo* (as in a B-DNA) in the rest of the DNA backbone (Fig. 4B).

All of the amide bonds of the PNA backbone are in the *trans* conformation and no intrabackbone hydrogen bonds are observed. Backbone torsion angles of the PNA monomers are reported in Table 5. Analysis of the values observed indicates that conformations of the PNA residues are highly conserved along the skeleton with some exceptions for the  $\alpha$  and  $\varepsilon$  angles. The variability in the latter angles causes changes in orientation of the backbone amide bond, without major displacement of the nucleobases. In particular, seven of the backbone carbonyl groups point toward the solvent, whereas the remaining two point in the opposite direction. In contrast, all of the carbonyl oxygens of the carboxymethyl moiety linker point toward the C-terminal direction of the PNA backbone,

**Table 2. Selected helical parameters**

Global base–base	$x$ -displacement, Å	Inclination, °	Local inter-base pair	Twist, °	Roll, °	Slide, Å
A1–Tpn10	–3.81	2.70	A1–Tpn10/G2–Cpn9	26.55	2.84	–2.41
G2–Cpn9	–4.13	–5.94	G2–Cpn9/T3–Apn8	28.84	–0.53	–2.03
T3–Apn8	–4.41	–8.40	T3–Apn8/G4–Cdl7	22.60	4.16	–2.31
G4–Cdl7	–4.38	–8.28	G4–Cdl7/A5–Tdl6	18.37	–1.54	–3.03
A5–Tdl6	–3.16	–5.77	A5–Tdl6/T6–Adl5	26.48	–6.85	–2.86
T6–Adl5	–3.20	–6.80	T6–Adl5/C7–Gpn4	24.31	8.63	–1.83
C7–Gpn4	–4.01	–1.92	C7–Gpn4/T8–Apn3	24.45	–3.06	–2.52
T8–Apn3	–4.17	–4.64	T8–Apn3/A9–Tpn2	20.43	16.67	–1.58
A9–Tpn2	–3.94	–1.56	A9–Tpn2/C10–Gpn1	16.38	–5.50	–2.20
C10–Gpn1	–2.45	2.83				

The helical parameters were determined by using the program CURVES (30).

**Table 3. Helical parameters (average)**

Helix	Twist, °	Rise, Å	Displacement, Å	Bases per turn
LPD	23.2	3.5	-3.8	16
PNA-PNA (11-13)	19.8	3.2	-8.3	18
PNA <sub>2</sub> -DNA triplex (10)	22.9	3.4	-6.8	16
PNA-DNA (9)	28.0	3.3	-3.8	13
DNA-DNA A (31)	32.7	2.6	-4.5	11
DNA-DNA B (31)	36.0	3.4	-0.1	10

The helical parameters were determined by using CURVES (30).

generating a significant dipole. The side chains of the three Lys-based residues point toward the solvent, and are involved in packing interactions. In particular, the  $\epsilon$ -amino groups of D-Lys side chains form ion pairs with the oxygens of the phosphate groups of the nucleotides of a symmetry-related molecule. All these interactions are mediated by water molecules (Fig. 5B).

The LPD asymmetric unit contains 80 water molecules, which stabilize the structure. The distribution of solvent molecules is clearly dependent on puckering of the sugars. In particular, when the sugar moiety assumes a C3'-endo conformation, most of the water molecules are located in the major groove, and are H-bonded with nucleobases (purine-N7 or pyrimidine O4/N4) and with oxygens of the phosphate groups. Water molecules located in the minor groove are also stabilized by H-bonds with nucleobases (purine-N3 or pyrimidine O2). In particular, those bound to the PNA strand form a bridge between the nucleobases and the amides of the backbone (N or O depending on the orientation of the amide bond), as observed for the PNA-PNA structure (11-13).

**Comparison with Other PNA-Containing Complexes.** The superposition of LPD onto PNA-DNA, PNA-PNA, and the Watson-Crick strands of (PNA)<sub>2</sub>-DNA yields a rms deviation of 1.48, 1.03, and

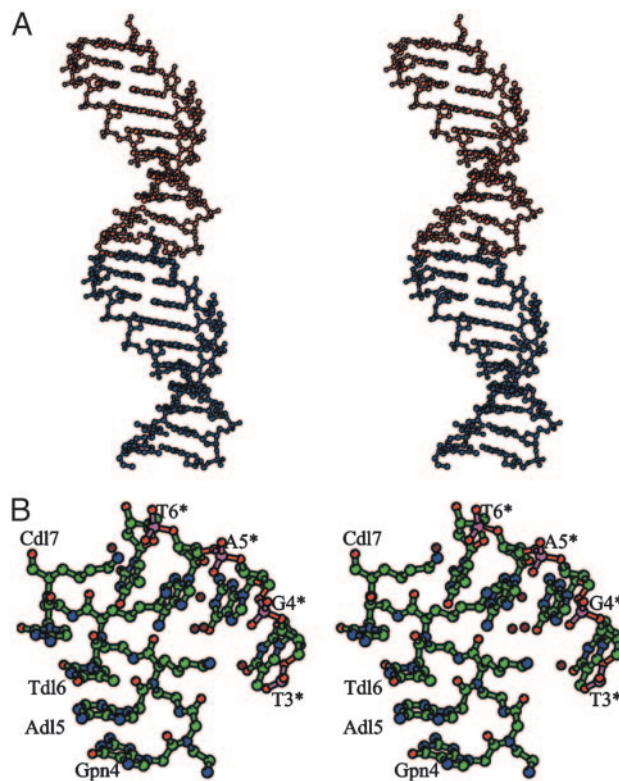


**Fig. 5.** Crystal-packing details. (A) A continuous base-pair stacking formed between the molecule in the asymmetric unit (in red) and a symmetry-related one (in blue). (B) Intermolecular electrostatic interactions occurring between D-Lys side chains of residues Adl5, Tdl6, and Cdl7 and phosphate groups of residues T3\*, G4\*, A5\*, and T6\*. The monomers with asterisks are related to the asymmetric unit by a 3<sub>1</sub> axis followed by a translation along the [1 1 0] direction. Water molecules are shown in dark red. The image was generated by using BOBSCRIPT (38).

0.92 Å, respectively, calculated on 12 corresponding carbon atoms directly linked to the nucleobase (C1' for the DNA and C8' for PNA). On the basis of these values, the LPD structure seems to resemble the PNA-PNA and (PNA)<sub>2</sub>-DNA structures more than the PNA-DNA structure. In particular, the mean twist angle and the number of bases per turn of LPD are consistent with those of the (PNA)<sub>2</sub>-DNA triplex (Table 3).

PNA monomer torsion angle values in LPD are consistent with those found in the PNA-PNA and (PNA)<sub>2</sub>-DNA structures (Table 5). Differences are observed only for the  $\alpha$  and  $\epsilon$  dihedral angles as a consequence of the two possible orientations of the amide bond of the backbone (as discussed above). In contrast, larger deviations concerning the  $\alpha$ ,  $\beta$ ,  $\delta$ , and  $\epsilon$  angles are observed in the PNA monomer conformation of the LPD structure as compared with the PNA-DNA determined by NMR (Table 5). Significant differences with respect to the PNA-DNA solution structure are present also in the DNA strands and, in particular, in the nucleotide torsion angles and in the conformation of the sugar rings. In fact, whereas in our structure the deoxyribose sugars present both C2'-endo (in four residues) and C3'-endo (in six residues) conformations, in the PNA-DNA structure determined in solution they are predominantly near the C2'-endo range. The sugar puckering is also different from that observed in the triplex structure, which is always in the C3'-endo conformation.

## Discussion

The analysis of the x-ray structure of the LPD duplex containing a chiral box in the middle of the sequence accomplishes two

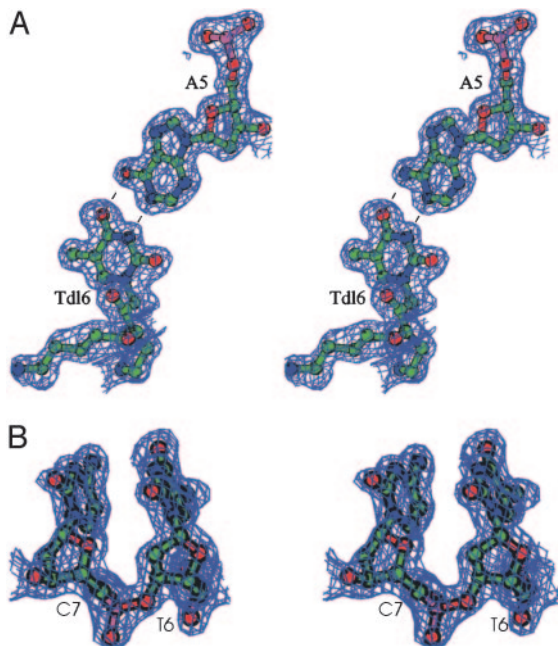


**Fig. 4.** Simulated annealing omit  $|2F_o - F_c|$  electron density map, computed at 1.66 Å and contoured at 1.0  $\sigma$ . (A) Representative Tdl6-A5 base pair engaged in Watson-Crick hydrogen bonds. (B) DNA residue T6 and C7 with the sugar moieties in the C3'-endo and C2'-endo conformation, respectively. The image was generated by using BOBSCRIPT (38).

**Table 4. DNA torsion angles per residue of LPD duplex**

Monomer	$\alpha$	$\beta$	$\gamma$	$\delta$	$\epsilon$	$\zeta$	$\chi$	Pseudorotation <i>P</i>
A1	-63.2	172.5	-151.5	88.8	-149.3	-77.4	-168.0	3.9
G2	-61.3	176.3	56.5	86.7	-155.1	-78.7	-168.1	17.0
T3	-65.8	178.0	48.1	83.4	-161.7	-72.8	-158.4	16.0
G4	144.6	-164.3	50.8	75.9	-167.2	-69.6	-158.2	22.1
A5	-55.2	175.5	-164.8	85.1	-155.3	-72.3	179.3	11.1
T6	-60.0	-174.4	53.5	84.5	-156.0	-78.1	-165.7	16.6
C7	-56.6	-161.4	55.2	141.1	173.0	-97.3	-121.6	160.1
T8	-5.32	-176.0	43.8	140.0	-144.9	-101.5	-121.4	155.9
A9	-95.0	78.0	-51.7	151.3	-168.8	-78.9	-89.3	165.6
C10			-179.2	145.0			-166.9	154.0
A-DNA* (10)	-50	172	41.1	79	-146	-78	-154	20.0
B-DNA* (10)	-46	-147	36	157	155	-96	-98	153.0
(PNA) <sub>2</sub> -DNA* (10)	-70	173	61	77	-161	-69	-167	19.5
PNA-DNA* (9)	-71	-165	49	110	-171	-75	-134	93.3

\*Average torsion angles.

important tasks. First, our results add further structural insights into PNA–DNA hybrids; second, the binding properties of PNAs containing a chiral box can now be discussed at a structural level.

The structural knowledge of PNA–DNA hybrids is currently based on a very limited number of cases. The (PNA)<sub>2</sub>-DNA triplex structure (10) showed helical parameters significantly different from those of canonical DNA or RNA helical forms, giving rise to a new class of helices called P-helices. The PNA–DNA solution structure (9) emphasized that the conformational features of the duplex fall in between those of canonical DNA structures (A- and B-DNA) and those of the P-helices. Finally, the solid state structure of a PNA–PNA duplex (11–13) was also found to belong to the P-type helix, suggesting that the P-helix could be the preferred conformation for PNAs.

The LPD structure presents a larger helical pitch, a wider and deeper major groove, and a narrower and shallower minor groove with respect to canonical A- and B-helical forms; thus it can be safely classified as a P-type double helix.

Dealing with the backbone conformation of the PNA strand, a detailed analysis of the LPD structure reveals that the dihedral angles of each monomer within the PNA strand are highly conserved along the sequence, except for the  $\alpha$  and  $\epsilon$  dihedral angles, which can determine two possible orientations of the amide bond in the backbone (see Table 5). In addition, the comparison between the LPD helix and those described in the literature reveals that all PNA torsion angles in LPD are very similar to those of the PNA–PNA duplex and of the (PNA)<sub>2</sub>-DNA triplex, whereas they show some differences with respect to those of the PNA–DNA duplex (see Table 5). On the other hand, if the local conformation of the DNA strand in the LPD duplex is considered, an unexpected variability in the sugar pucker is observed. In particular, sugar moieties within segment 1–6 are endowed with a C3'-endo conformation (A-like), whereas the sugars in segment 7–10 adopt a C2'-endo conformation (B-like). The former conformation seems to be stabilized by packing electrostatic interactions (see above). It is worth noting that in the (PNA)<sub>2</sub>-DNA structure all of the sugar moieties are found in the C3'-endo conformation, whereas in the PNA–DNA duplex they show a predominant C2'-endo conformation with minor contributions from the C3'-endo form. Taken together, these findings suggest that the P-helix can accommodate both sugar conformations and that environmental conditions can stabilize one with respect to the other. This fact and the substantial similarity between the PNA conformation in LPD and the conformations observed in other PNA structures reinforce the view that in double helices the flexibility of the PNA strand is rather restricted despite the absence of cyclic moieties, and that PNAs possess intrinsic conformational preferences for the P-helix. The DNA

moiety then becomes adapted to the PNA P-helix conformation rather than vice versa. These conclusions are in agreement with molecular dynamics studies (32–33) and with the “constrained flexibility” concept developed for PNAs and their analogues (16), whereas they reverse the early concept of PNAs as molecules endowed with high conformational adaptability (9).

The introduction of sterically hindered chiral centers in the PNA backbone may be envisaged as further restricting the adaptability of PNA to the DNA strand. As a matter of fact, in terms of groove sizes, pitch, and twist parameters, the LPD double helix more closely resembles that of the PNA–PNA homoduplex than that of the achiral PNA–DNA heteroduplex. However, it is not clear whether the structural differences between LPD and the PNA–DNA double helix arise entirely from the conformational restraints brought about by the presence of the chiral box in the PNA backbone, or whether they arise from the different experimental conditions (crystal versus solution, different length and base sequences). It must be emphasized that the structure of PNA–DNA has been obtained in solution, therefore being sensitive to conformational averaging processes. To address this point, it could be useful to determine the crystal structure of the achiral homologue of LPD.

The steric hindrance due to the bulky D-Lys side chains and the consequent rigidity of chiral PNA strands may explain a number of properties of the corresponding hybrids with DNA. The preference of chiral PNAs to form right-handed helical structures was evaluated by forming duplexes with complementary achiral PNAs (18, 22). D-amino acid-containing PNAs (especially those bearing charged side chains) were shown to promote the formation of right-handed structures. This finding is supported by another study, based on the interaction of cyanine dyes with PNA–PNA duplexes

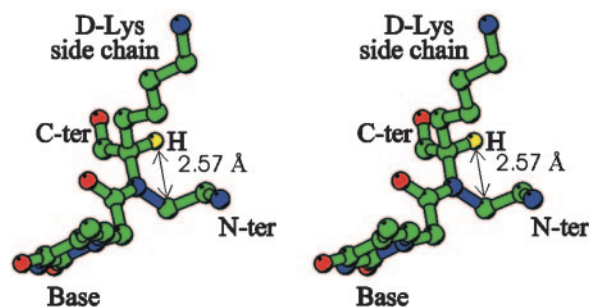


**Fig. 6.** Stereoview of residue Tdl6, showing the interaction between the hydrogen atom (in yellow) bound to the chiral center and the C3' atom. The image was generated by using BOBSCRIPT (38).

**Table 5. PNA torsion angles per residue of LPD duplex**

Monomer	$\alpha$	$\beta$	$\gamma$	$\delta$	$\varepsilon$	$\omega$	$\chi^1$	$\chi^2$	$\chi^3$
Gpn1		-47.6	-65.0	111.4	-30.1	176.7	-0.1	175.8	-106.3
Tpn2	66.9	81.4	59.2	94.4	-20.7	176.3	0.2	-179.6	-93.4
Apn3	76.6	72.8	67.8	88.1	174.5	-177.0	10.2	-177.4	-97.8
Gpn4	-98.9	58.6	72.4	83.2	-171.4	-176.9	0.9	-170.4	-85.3
Adl5	-130.6	74.1	70.3	86.7	-170.3	-178.1	16.5	-180.0	-98.8
Tdl6	-132.4	79.6	68.1	90.3	-179.9	-177.5	1.4	178.6	-95.0
Cdl7	-115.9	71.5	69.0	87.4	178.7	-177.8	1.9	180.0	-87.3
Apn8	-100.5	60.8	67.5	100.2	158.8	-176.6	0.9	-175.9	-83.6
Cpn9	-107.9	82.7	64.7	90.0	179.5	-179.3	0.7	-178.2	-90.3
Tpn10	-98.0	59.8	64.6	91.2	153.8		0.6	-178.2	-75.7
Watson-Crick PNA triplex* (10)	-103	73	70	93	165		1	-175	89
PNA-DNA* (9)	105	141	78	139	35		-3	151	-103
PNA-PNA* (11)	-118 (83) <sup>†</sup>	64	75	88	171 (21) <sup>†</sup>		7	-175	83

Scheme for torsion angle definitions:  $\alpha = C'-N1'-C2'-C3'$ ;  $\beta = N1'-C2'-C3'-N4'$ ;  $\gamma = C2'-C3'-N4'-C5'$ ;  $\delta = C3'-N4'-C5'-C'$ ;  $\varepsilon = N4'-C5'-C'-O1'$ ;  $\omega = C5'-C'-N-C2'$ ;  $\chi^1 = C3'-N4'-C7'-C8'$ ;  $\chi^2 = N4'-C7'-C8'-N1/N8$ ; and  $\chi^3 = C6'-C7'-N1/N8-C2/C4$ .

\*Average torsion angles.

<sup>†</sup>Two alternative values of  $\alpha$  and  $\varepsilon$  angles are found, corresponding to different orientations of the backbone amide bond.

(19). In agreement with this preference, PNAs containing D-amino acids were found to form more stable complexes with right-handed DNA. By analyzing the LPD structure, it can be seen that the observed preference for right-handedness is not induced by any specific interaction between the PNA side chains and the DNA backbone; instead, an intrastrand repulsive van der Waals interaction occurs between the D-Lys side chain and the aminoethyl group (Fig. 6). We observed that, if the configuration of a Lys residue of LPD is changed from D to L, a large variation of the  $\delta$  dihedral angle must occur to minimize steric overlap. Instead, it has been experimentally found that  $\delta$  dihedral angle values are highly conserved in PNAs.

The higher rigidity of the D-Lys-containing PNA may be also related to the ability of LPD in discriminating mismatches in the target antiparallel DNA strand. It is known that the presence of mispairings in the double helices induces small distortions in the backbone conformation, leading to formation of the so-called “wobble structures” (35–37). The decrease in the backbone flexibility could hamper the conformational rearrangements necessary to accommodate the mispairs in the double helix.

In conclusion, the results presented herein indicate that the introduction of chiral centers in the middle of a PNA backbone does not alter significantly the tendency of PNAs to form P-like helices when complexed with complementary DNA strands. However, it can limit the ability of the PNA strands to adopt other conformations, thus increasing the recognition selectivity.

As a final remark, it is observed that the free amino groups inserted in this way do not alter the global structure of PNA-DNA duplexes. Thus, C5'-substituted PNAs may represent a powerful strategy to insert functional groups to be further conjugated with suitable compounds and to achieve PNA derivatives endowed with enhanced properties as antigene/antisense therapeutics or as reporters for specific applications in diagnostics.

We thank Maurizio Amendola and Giosuè Sorrentino for technical assistance, Sincrotrone Trieste Consiglio Nazionale delle Ricerche/Elettra for giving us the opportunity to collect data at their crystallographic beamline, and the European Synchrotron Radiation Facility for providing the synchrotron radiation facilities and for assistance in using Beamline ID14-1. This work was supported by the Ministero dell'Istruzione, dell'Università e della Ricerca (Contributo Straordinario Decreto 4-10-2001) and the Italian National Research Council.

- Nielsen, P. E., Egholm, M., Berg, R. H. & Buchardt, O. (1991) *Science* **254**, 1497–1500.
- Egholm, M., Buchardt, O., Christensen, L., Behrens, C., Freier, S. M., Driver, D. A., Berg, R. H., Kim, S. K., Norden, B. & Nielsen, P. E. (1993) *Nature* **365**, 566–568.
- Uhlmann, E., Peyman, A., Breipohl, G. & Will, D. W. (1998) *Angew. Chem. Int. Ed. Engl.* **37**, 2796–2893.
- Nielsen, P. E. (2000) *Curr. Opin. Mol. Ther.* **2**, 282–287.
- Ray, A. & Norden, B. (2000) *FASEB J.* **14**, 1041–1060.
- Cutrona, G., Carpaneto, E. M., Ulivi, M., Roncella, S., Landt, O., Ferrarini, M. & Boffa, L. C. (2000) *Nat. Biotechnol.* **18**, 300–303.
- Nielsen, P. E. (2001) *Curr. Opin. Biotechnol.* **12**, 16–20.
- Brown, S. C., Thomson, S. A., Veal, J. M. & Davis, D. G. (1994) *Science* **265**, 777–780.
- Eriksson, M. & Nielsen, P. E. (1996) *Nat. Struct. Biol.* **3**, 410–413.
- Betts, L., Josey, J. A., Veal, J. M. & Jordan, S. R. (1995) *Science* **270**, 1838–1841.
- Rasmussen, H., Kastrop, J. S., Nielsen, J. N., Nielsen, J. M. & Nielsen, P. (1997) *Nat. Struct. Biol.* **4**, 98–101.
- Haaima, G., Rasmussen, H., Schmidt, G., Jensen, D. K., Kastrop, J. S., Stafshede, P. W., Nordén, B., Buchardt, O. & Nielsen, P. E. (1999) *New J. Chem.* **23**, 833–840.
- Eldrup, A. B., Nielsen, B. B., Haaima, G., Rasmussen, H., Kastrop, J. S., Christensen, C. & Nielsen, P. E. (2001) *Eur. J. Org. Chem.* **9**, 1781–1790.
- Gildea, B. D., Casey, S., MacNeill, J., Perry-O'Keefe, H., Sorensen, D. & Coull, J. (1998) *Tetrahedron Lett.* **39**, 7255–7258.
- Soomets, U., Häällbrink, M. & Langel, U. (1999) *Front. Biosci.* **4**, D782–D786.
- Ganesh, K. N. & Nielsen, P. E. (2000) *Curr. Org. Chem.* **4**, 916–928.
- Haimaa, G., Lohse, A., Buchardt, O. & Nielsen, P. E. (1996) *Angew. Chem. Int. Ed. Engl.* **35**, 1939–1942.
- Sforza, S., Haaima, G., Marchelli, R. & Nielsen, P. E. (1999) *Eur. J. Org. Chem.* **197**–204.
- Smith, J. O., Olson, D. A. & Armitage, B. A. (1999) *J. Am. Chem. Soc.* **121**, 2686–2695.
- Sforza, S., Corradini, R., Ghirardi, S., Dossena, A. & Marchelli, R. (2000) *Eur. J. Org. Chem.* **2905**–2913.
- Menchise, V., De Simone, G., Corradini, R., Sforza, S., Sorrentino, N., Romanelli, A., Saviano, M. & Pedone, C. (2002) *Acta Crystallogr. D* **58**, 553–555.
- Sforza, S., Tedeschi, T., Corradini, R., Ciavardelli, D., Dossena, A. & Marchelli, R. (2003) *Eur. J. Org. Chem.*, 1056–1063.
- Otwinowski, Z. & Minor, W. (1997) *Methods Enzymol.* **276**, 307–326.
- Terwilliger, T. C. & Berendzen, J. (1997) *Acta Crystallogr. D* **53**, 571–579.
- Collaborative Computational Project No. 4 (1994) *Acta Crystallogr. D* **50**, 760–763.
- Cowtan, K. D. & Main, P. (1998) *Acta Crystallogr. D* **54**, 487–493.
- Jones, T. A., Zou, J. Y., Cowan, S. W. & Kjeldgaard, M. (1991) *Acta Crystallogr. A* **47**, 110–119.
- Read, R. J. (1986) *Acta Crystallogr. A* **42**, 140–149.
- Brünger, A. T., Adams, P. D., Clore, G. M., DeLano, W. L., Gros, P., Grosse-Kunstleve, R. W., Jiang, J. S., Kuszewski, J., Nilges, M., Pannu, N. S., et al. (1998) *Acta Crystallogr. D* **54**, 905–921.
- Lavery, R. & Sklenak, H. (1988) *J. Biomol. Struct. Dyn.* **6**, 63–91.
- Bloomfield, V. A., Crothers, D. M. & Tinoco, I., Jr., eds. (2000) *Nucleic Acids: Structures, Properties, and Functions* (Univ. Sci. Books, Mill Valley, CA), pp. 88–91.
- Sen, S. & Nilsson, L. (1998) *J. Am. Chem. Soc.* **120**, 619–631.
- Soliva, R., Sherer, E., Luque, F. J., Laughton, C. A. & Orzco, M. (2000) *J. Am. Chem. Soc.* **122**, 5997–6008.
- Sforza, S., Galaverna, G., Dossena, A., Corradini, R. & Marchelli, R. (2002) *Chirality* **14**, 591–598.
- Ramakrishnan, B. & Sundaralingam, M. (1995) *J. Mol. Biol.* **246**, 194–208.
- Wahl, M. C. & Sundaralingam, M. (1997) *Biopolymers* **44**, 45–63.
- Allawi, H. T. & SantaLucia, J. (1998) *Nucleic Acids Res.* **26**, 4925–4934.
- Esnouf, R. M. (1999) *Acta Crystallogr. D* **55**, 938–940.